SCIPEDIA Revista Internacional de Métodos Numéricos para Cálculo y Diseño en Ingeniería

Revista Internacional Métodos numéricos para cálculo y diseño en ingeniería RIMNI

in cooperation with CIMNE

An Enhanced Pilot Aided Channel Estimation in XL-MIMO Communication Systems Using Bitterling Swallow Fish Optimization

Mian Muhammad Kamal[1,*], Syed Zain Ul Abideen[2], Yinsheng Luo[1], Abdelrahman Hamza Hussein[3], Husam S. Samkari[4,5], Mohammed F. Allehyani[4] and Tianjun Ma[1,*]

[1]School of Electronics and Communication Engineering, Quanzhou University of Information Engineering, Quanzhou, 362000, China

[2]College of Mechatronics and Control Engineering, Shenzhen University, Shenzhen, 518060, China

[3]Department of Networks and Cybersecurity, Hourani Center for Applied Scientific Research, Al-Ahliyya Amman University, Amman, 19111, Jordan

[4]Department of Electrical Engineering, University of Tabuk, Tabuk, 47713, Saudi Arabia

[5]Artificial Intelligence and Sensing Technologies Research Center, University of Tabuk, Tabuk, 47713, Saudi Arabia

ABSTRACT

The continuous evolution of 6th Generation (6G) wireless networks places Extremely Large-scale Multiple-Input Multiple-Output (XL-MIMO) schemes as a crucial enabler for ultra-reliable and high data rate communication. Channel estimation in XL-MIMO is crucial here because it allows the system to precisely recognize the wireless channel conditions between the transmitter and receiver, which is vital for enhancing signal processing, and resource allocation. Traditional pilot-aided channel estimation approaches face challenges, such as high error. Hence, this work proposes an innovative model called the Deep Kronecker Network-Bitterling Swallow Fish Optimization Algorithm (DKN-BSwaFOA) for pilot-aided channel estimation in XL-MIMO systems. Initially, the system model of XL-MIMO is contemplated. The pilot insertion is done at the transmitter, and the location of the pilot symbol is optimally selected using BSwaFOA. The signal is propagated over the hybrid field channel, where both far-field and near-field components coexist. At the receiver, the channel is estimated using DKN, which is trained using the proposed BSwaFOA. The experimental outcomes demonstrated that the DKN_BSwaFOA computed the minimum Root Mean Square Error (RMSE), Bit Error Rate (BER), and Mean Square Error (MSE) of 0.030, 0.002, and 0.001.

OPEN ACCESS

Received: 23/09/2025

Accepted: 11/11/2025

DOI
10.23967/j.rimni.2025.10.73668

Keywords:
Extremely large-scale-multiple-input-multiple-output
channel estimation
pilot insertion
deep learning
optimization

1 Introduction

Wireless communication is becoming an integral part of modern life with the unprecedented deployment and evolution over the past few decades, and it also provides the foundation for countless services and applications. Wireless communication technologies have increased dramatically

*Correspondence: Mian Muhammad Kamal, Tianjun Ma (mianmuhammadkamal@qzuie.edu.cn, matianjun@qzuie.edu.cn).

in communication coverage, reliability, and throughput from the basic voice calls on 1st Generation (1G) networks to reliable and fast video streaming performed by the 5th Generation (5G) networks. Meanwhile, the present wireless infrastructure failed to meet the basic requirements of the 6G network [1]. As network densification is unattractive commercially, a larger number of antennas is exploited by the base stations (BS) to support more traffic. Thus, the next-generation MIMO technologies are utilized for deploying an extremely large number of antennas [2]. In the 6G era, the key enablers are identified by using two groundbreaking wireless innovations to achieve high data rates. The XL-MIMO is the first innovation, which is characterized by deploying a large array of antennas at the BS, and the XL-MIMO significantly increases the spectral efficiency. Similarly, the Terahertz (THz) bands or millimeter wave (mmWave) are the second one that helps to enhance the carrier frequencies, which also provides a substantial number of available unlicensed bandwidth [3]. XL-MIMO systems are an emerging key technology for future wireless systems that help to increase spectral efficiency and spatial resolutions by significantly leveraging a large number of antenna elements [4]. In future 6G communications, the XL-MIMO is used to attain 10-fold increases in spectral efficiency [5].

Ideally, XL-MIMO effectively mitigates various challenges encountered by classical massive MIMO systems due to the deployment of thousands or hundreds of antennas [6]. XL-MIMO systems generally increase the positioning accuracy by leveraging beamforming gains and spatial multiplexing and are expected to attain high energy and spectrum efficiencies [7]. In beamforming, the XL-MIMO generates a directional beam with high array gain to get spatial multiplexing gain. In XL-MIMO, the channel estimation is performed to accumulate Channel State Information (CSI) before realizing beamforming [8–10]. Moreover, the XL-MIMO performs comprehensive channel estimation and increases multi-user communications to acquire the complete information of channel states [11,12]. Meanwhile, the increasing number of BS antennas leads to the unaffordable pilot overhead while estimating channel states from high-dimensional XL-MIMO. The low-overhead channel estimation schemes are generally categorized into two types, namely, near-field channel estimation and far-field channel estimation. In near-field channel estimation, the channel sparsity in the polar domain is considered, and the propagation offers various stringent challenges and valuable opportunities while designing the transceiver. Likewise, the channel sparsity in the angle domain is considered in the far-field channel estimation [9,13]. Nowadays, the pilot-aided channel estimation is performed by multiplexing known training symbols with data to get CSI. The channel estimates are generated exclusively using pilot symbols in pilot-aided channel estimation, and the estimates are processed to detect data symbols based on the channel response [14,15].

In XL-MIMO, the traditional channel estimation methods, like Least Squares (LS) and Minimum Mean Square Error (MMSE), are extended directly with fully digital precoding and Time Division Duplex (TDD)-based XL-MIMO systems. The TDD systems with hybrid precoding are widely utilized in XL-MIMO for reducing the total frequency chains and Frequency Division Duplex (FDD) systems [11]. Moreover, the prevailing XL-MIMO channel estimation techniques are similar to the algorithms used by far-field hybrid antenna arrays, which helps to estimate the parameters used by the channels [14,16,17]. Contrarily, the compressive sensing-based channel estimation techniques mainly rely on angular sparsity, which also results in experiencing a significant loss of performance in XL-MIMO systems. Thus, various studies are followed for capturing the sparsity among the inherent joint angle-distance available in the near-field channel to address these challenges [18,19]. Recently, various researchers have performed extensive research using channel estimation algorithms to explore different characteristics of XL-MIMO channels [7]. Furthermore, extensive works are conducted to explore the sparse structure of THz and mmWave channels for introducing channel estimation algorithms with minimum pilot overhead [20]. Also, Deep learning (DL)-based channel

estimation algorithms have been used in recent years to gain significant momentum [21]. Nowadays, DL-based techniques are gradually utilized for advanced transceiver design. The DL techniques help to effectively tackle the issues encountered by near-field XL-MIMO systems. Moreover, DL techniques effectively increased the performance of different transceiver modules by utilizing the high-dimensional channel distribution [9].

This research designs an innovative approach, DKN-BSwaFOA, for pilot-aided channel estimation in XL-MIMO systems. Firstly, the system model of XL-MIMO is contemplated. At the transmitter, the input signal undergoes S/P conversion. After this, pilot insertion is carried out, and the location of the pilot symbol is optimally selected exploiting BSwaFOA. Here, the BSwaFOA is designed by incorporating the House Swallow Optimizer (HSO) and Bitterling Fish Optimization (BFO). Later, the Inverse Fast Fourier Transform (IFFT) is applied for converting the frequency domain signal to the time domain. Following this, a Cyclic Prefix (CP) is added to mitigate Inter-Symbol Interference (ISI). The signal is then converted back to serial form via parallel to serial (P/S) conversion and transmitted over a hybrid field channel, where near-field and far-field effects coexist. At the receiver phase, the signal first undergoes serial-to-parallel (S/P) conversion, followed by CP removal. The resulting signal is then transformed back to the frequency domain through FFT. Later, P/S conversion is applied, and then the pilot-aided channel estimation is done employing the DKN, which is trained with BSwaFOA.

The prime contribution of this work is listed below,

- ***Introduced DKN_BSwaFOA for pilot-aided channel estimation in XL-MIMO systems:*** Here, pilot insertion is carried out at the receiver, and the location of the pilot symbols is optimally selected exploiting BSwaFOA. Here, the BSwaFOA is designed by incorporating the HSO and BFO. Furthermore, the pilot-aided channel estimation is done employing the DKN, which is trained with BSwaFOA.

The structural arrangement of the residual section of this research is as follows: Section 2 provides the motivation, and literature review of existing pilot-aided channel estimation approaches with their pros and cons, Section 3 specifies the system model of XL-MIMO, Section 4 deliberates the devised DKN_BSwaFOA for pilot-aided channel estimation, Section 5 explicates the experimental outcomes and comparative assessment, and Section 6 concludes the works with future directions.

2 Motivation

Pilot-aided channel estimation is a fundamental approach in wireless communication schemes, where known pilot symbols are inserted into the transmitted signal to enable precise estimation of the CSI at the receiver. Nevertheless, existing techniques frequently suffer from significant limitations, including high pilot overhead that minimizes spectral efficacy, poor performance in fast-fading or time-varying channels, and susceptibility to noise and interference. These difficulties become more pronounced in advanced situations, like high-mobility environments, XL-MIMO, and next-generation networks, such as 5G and 6G. Hence, there is a crucial need to improve pilot-aided channel estimation by establishing more effective, adaptive, and robust models that can deliver high estimation accuracy with minimized pilot overhead. Hence, this work proposes an efficient approach called DKN_BSwaFOA for pilot-aided channel estimation in XL-MIMO systems.

2.1 Literature Survey

Jin et al. [3] presented a Non-Markovian Generative Diffusion Model (NM-GDM) for near-field channel estimation. This approach enhanced generalizability and was robust in performing the channel estimation task under limited communication overhead. However, this model failed to increase the sampling efficiency and optimize the model for lightweight design to enable the deployment of GDM in wireless communication networks. Ye et al. [5] developed IE-Pix2pix for near-field channel estimation. The IE-Pix2pix effectively learned the adversarial losses and attained high performance under less pilot overhead and minimum pilot length. Still, this model was not successful for real-time channel estimation in XL-MIMO communication systems. Liu et al. [22] devised Discrete Prolate Spheroidal Sequences (DPSS) for near-field channel estimation in XL-MIMO systems. The DPSS model recorded minimum computational complexities while accurately estimating the location of scatters and users, which also estimated CSI in real-world scenarios with minimum training overhead and hardware requirements. Meanwhile, this approach recorded high computational time for efficient near-field channel estimation. Cui and Dai [20] established Bilinear Pattern Detection (BPD) for near-field wideband channel estimation. This technique significantly accumulated the bilinear patterns to successively identify the channel paths and also accurately estimated the physical location of each path. But the BPD failed to tackle the relevant channel estimation issues in different near-field wideband communication scenarios, like cell-free massive MIMO communications and Reconfigurable Intelligent Surface (RIS) communications.

Lei et al. [21] introduced Polar-Domain Multi-Scale Residual Dense Network (P-MSRDN) for channel estimation for XL-MIMO systems. This approach recorded minimum channel sparsity issues and effectively addressed the inherent performance loss during channel estimation in XL-MIMO systems. Still, this model was not successful for XL-MIMO systems under hybrid-field scenarios by considering that different user equipments is in the near-field. Gao et al. [23] established a Compressed XL-MIMO channel network (C-XLCNet) for channel estimation in XL-MIMO systems. The C-XLCNet model incurred limited performance loss while minimizing computational complexities and storage space for the estimation of high-dimensional channels. However, this approach failed to perform additional weight quantization operations for channel estimation, thereby mitigating the aggravated issues concerning the channel prior knowledge and computation load. Lei et al. [24] devised Hybrid-field Stochastic Gradient Pursuit (SGP) for channel estimation in XL-MIMO. The Hybrid-field SGP was robust and resilient against noise and recorded low complexities with higher achievable rates in channel estimation. Nevertheless, this model failed to consider the impacts of the EM polarization property and spatial non-stationary characteristics in estimating the performance of XL-MIMO systems. Tang et al. [25] presented a Sparse Bayesian Learning-Graph Neural Network (SBL-GNN) for channel estimation for XL-MIMO systems. The SBL-GNN scheme significantly increased the robustness and accuracy in channel estimation by capturing the dependencies among channel coefficients under the lowest runtime and low pilot overhead. Though, this scheme recorded a high computational cost during the estimation of channel state in XL-MIMO systems. A comparative analysis of pilot-aided channel estimation techniques in XL-MIMO systems is provided in Table 1.

Table 1: Comparative analysis of pilot-aided channel estimation techniques in XL-MIMO systems

Ref.	Techniques	Key idea/focus	Advantages	Disadvantages	Key performance (RMSE/BER)	Computational complexity	Robustness to noise & interference	Pilot overhead reduction	Supported channel scenarios
[3]	NM-GDM	Deep generative model using side information	High generalizability, robust with low overhead	High memory/latency, no advanced compression	Moderate	High (due to iterative diffusion process)	High	Moderate	Near-field
[5]	IE-Pix2pix	GAN-based estimation Fast convergence, low pilot length	Rapidly converges with shorter pilots and better performance	Lacked robustness in diverse channels	Good	Moderate (GAN-based training)	Moderate	High	Near-field
[22]	DPSS	Sensing-enhanced with prolate sequences	Minimized pilot overhead via optimal error estimation	Poor generalization to complex scenarios	Good	Low	High	High	Near-field
[20]	BPD	Bilinear pattern detection for path identification	High accuracy in various domains	High tuning needs, no real-world validation	Excellent	Moderate to High	Moderate	Moderate	Hybrid-field
[21]	P-MSRDN	Deep network exploiting polar-domain sparsity	High generalization, effective sparsity use	Sensitive to hyperparameters, suboptimal tuning	Very Good	High (Deep Network)	High	Moderate	Near-field
[23]	C-XLCNet	Compressed & pruned deep network	Low runtime and parameters, fast convergence	Lacks real-world robustness	Good	Moderate (after pruning)	Moderate	High	General XL-MIMO
[24]	Hybrid-field SGP	Stochastic gradient pursuit for hybrid fields	High achievable rates, improved accuracy	Computational overhead, slow for real-time	Very Good	Low to Moderate	High	Moderate	Hybrid-field
[25]	SBL-GNN	Sparse Bayesian Learning enhanced with GNNs	Computationally effective, accurate	Slow convergence, sensitive to initialization	Excellent	Moderate (GNN integration)	High	High	XL-MIMO (General)

(Continued)

Table 1 (continued)

Ref.	Techniques	Key idea/focus	Advantages	Disadvantages	Key performance (RMSE/BER)	Computational complexity	Robustness to noise & interference	Pilot overhead reduction	Supported channel scenarios
Proposed Work	**DKN_BSwaFOA**	**Hybrid metaheuristic-optimized deep Kronecker network**	**Optimal pilot selection, superior hybrid-field accuracy**	**High computational complexity, idealistic assumptions**	**Excellent**	**High (Hybrid Metaheuristic + Deep Network)**	**High (Optimized training)**	**High**	**Hybrid-field**

2.2 Major Challenges

The key difficulties encountered by the existing techniques of pilot-aided channel estimation in XL-MIMO are as follows:

- The BPD algorithm developed in [20] recovered each near-field channel path by utilizing the bilinear pattern for the accumulation of the largest polar-domain power from the entire bandwidth. However, this scheme failed to resolve multi-path components more precisely, which would have enhanced channel estimation accuracy, particularly in rich scattering environments.
- The P-MSRDN scheme in [21] exploited near-field channel sparsity in the polar domain during channel estimation. Though this model failed to reduce interference during secondary user access in cognitive radio setups.
- The C-XLCNet framework, designed in [23], effectively mitigated the aggravated issues based on the dependence on channel prior knowledge and computation load. Meanwhile, this technique failed to minimize sensing latency in ultra-dense or fast-changing environments.
- In [25], the SBL-GNNs network employed an SBL approach enhanced by GNNs, where the dependencies among channel coefficients were captured by retaining the E-step of the traditional SBL algorithm and updating the M-step with GNNs. But this approach failed to enable low-complexity time-domain transmission, which would have been energy-efficient for large antenna arrays.
- Enhanced Channel Estimation and Dynamic Spectrum Access in XL-MIMO systems intelligently allocate spectrum resources in real time for channel estimation. However, real-time implementation faces challenges due to high-dimensional CSI overhead and rapidly changing spectrum conditions, necessitating innovative models that ensure low-latency, adaptive, and efficient communication.

3 System Model of XL-MIMO

In an XL-MIMO scheme [24], a point-to-point uplink communication scenario is contemplated under Time Division Duplexing (TDD) and hybrid field conditions, where the BS exploits a Uniform Linear Array (ULA) with ω_J elements, and User Equipment (UE) is equipped with ω_h antennas. The antenna spacing is represented by $\Delta = \frac{\zeta}{2}$, here carrier wavelength is signified as ζ. Let $Z \in \mathbb{C}^{\omega_J \times \omega_h}$ specifies channel among BS and UE. When the UE passes a pilot signal of length δ, the received signal

at the BS is typified by $\chi \in \mathbb{C}^{\omega_J \times \delta}$, and is stated as follows,

$$\chi = Z\beta\Phi^T + \tau \tag{1}$$

here, the precoding matrix exploited by the UE during the pilot transmission stage is signified as $\beta \in \mathbb{C}^{\omega_J \times \omega_h}$, the pilot matrix transmitted by the UE to BS is represented by $\Phi \in \mathbb{C}^{\delta \times \omega_h}$ such that $\Phi^T\Phi^* = \delta I_{\omega_h} = \tau \in \mathbb{C}^{\omega_J \times \delta}$ indicates additive noise at UE with independent and identical distributed entries $CN\left(0, w^2\right)$, where noise power is denoted as w and circularly symmetric complex Gaussian distribution is designated by CN. The precoding matrix is subject to an overall power constraint, requiring $tr\left(\beta\beta^H\right) = \eta$, wherein UEs' overall transmit power is signified by η and Hermitian transpose is signified by H.

The received signal is first compared with the normalized pilot matrix $\frac{\Phi^*}{\sqrt{\delta}}$ to acquire $\chi_m = \frac{1}{\sqrt{\delta}}\chi\Phi^* \in \mathbb{C}^{\omega_J \times \omega_h}$ at the BS, and is articulated as follows,

$$\chi_m = \frac{1}{\sqrt{\delta}}Z\beta\Phi^T\Phi^* + \frac{1}{\sqrt{\delta}}\tau\Phi^* = \sqrt{\delta}Z\beta + \tau_m \tag{2}$$

here, equivalent noise is specified by $\tau_m = \frac{1}{\sqrt{\delta}}\tau\Phi^* \in \mathbb{C}^{\omega_J \times \omega_h}$. Fig. 1 signifies the system model of hybrid field communication.

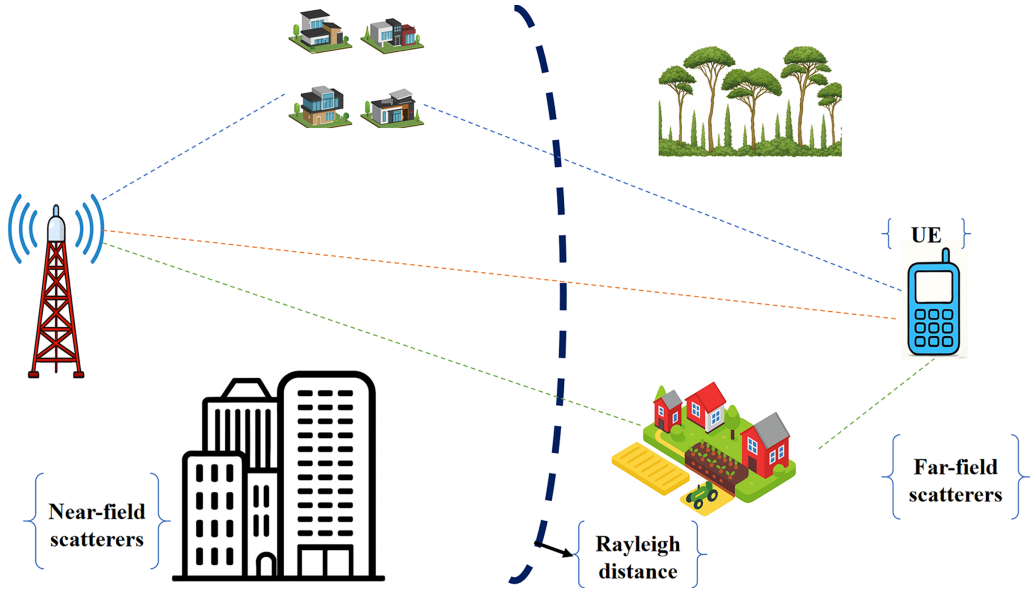

Figure 1: System model of XL-MIMO

Channel Model

In XL-MIMO schemes, the enlarged near-field area necessitates consideration of both near-field and far-field propagation effects. Accordingly, under a hybrid-field communication scenario, the XL-MIMO channel is modelled as the superposition of two different elements, namely the far-field component and near-field components. Due to the fundamental differences in wavefront features, spherical in the near-field and planar in the far-field, these components are modelled independently.

Without loss of generality, the channel is considered to consist of one dominant line-of-sight (LoS) path and $\varepsilon - 1$ non-line-of-sight (NLoS) paths. Based on the corresponding array response vectors, the hybrid-field XL-MIMO channel $Z \in \mathbb{C}^{\omega_J \times \omega_h}$ can be specified below:

$$Z = \begin{bmatrix} \sqrt{\omega_J \omega_h}\bar{\hbar}_0 G\left(N_{\kappa,0}, \theta_{\kappa,0}\right) G^H\left(N_{T,0}, \theta_{T,0}\right) \\ +\sqrt{\frac{\omega_J \omega_h}{\varepsilon - 1}} \sum_{C=1}^{\varepsilon-1} \hbar_C G\left(N_{\kappa,C}, \theta_{\kappa,C}\right) G^H\left(N_{T,C}, \theta_{T,C}\right) \\ \stackrel{(s)}{=} \sqrt{\frac{\omega_J \omega_h}{\varepsilon - 1}} \sum_{C=0}^{\varepsilon-1} \hbar_C G\left(N_{\kappa,C}, \theta_{\kappa,C}\right) G^H\left(N_{T,C}, \theta_{T,C}\right) \end{bmatrix} \tag{3}$$

wherein, overall amount of path components is signified by ε, distance among BS and UE is indicated as $N_{\kappa,0}$ and $N_{T,0}$, the LoS path is characterized by the array response vectors $\left(N_{\kappa,0}, \theta_{\kappa,0}\right) \in \mathbb{C}^{\omega_J \times 1}$ at the BS and $\left(N_{T,0}, \theta_{T,0}\right) \in \mathbb{C}^{\omega_h \times 1}$ at the UE, $\theta_{\kappa,0}$ signifies angle of LoS path at BS, $\theta_{T,0}$ specifies angle of LoS path at UE, path gain of LoS path is represented by $\bar{\hbar}_0$, the gain of the C^{th} NLoS path is designated as $\hbar_C$, the NLoS paths are typified by the array response vectors $G\left(N_{\kappa,C}, \theta_{\kappa,C}\right)$ at the BS and $G\left(N_{T,C}, \theta_{T,C}\right)$ at the UE.

(i) Far field channel

Among the whole ε paths, $\varepsilon_W = \lfloor \varpi \varepsilon \rfloor$ are assumed to be far-field components, where the tunable parameter is specified as $0 \leq \varpi \leq 1$. The far-field channel $Z_{far-field} \in \mathbb{C}^{\omega_J \times \omega_h}$ is then modeled based on the planar wavefront assumption and can be given as:

$$Z_{far-field} = \sqrt{\frac{\omega_J \omega_h}{\varepsilon - 1}} \sum_{C_M=1}^{\varepsilon W} \hbar_{C_M} G\left(\theta_{\kappa,C_M}\right) \; G^H\left(\theta_{T,C_M}\right) \tag{4}$$

Here, the gain of C^{th} the NLoS path is specified as $\hbar_C$. The angular-domain representation $Z^y_{far-field} \in \mathbb{C}^{\hbar_J \times \omega_h}$ of the far-field channel $Z_{far-field}$ can be obtained using a pair of Discrete Fourier Transform (DFT) matrices ψ_κ and ψ_T, as specified as follows,

$$Z_{far-field} = \psi_\kappa Z^y_{far-field} \psi_T^H \tag{5}$$

here, unitary matrices are specified as $\psi_\kappa = \left[s\left(\theta_1\right), \ldots, s\left(\theta_{d_J}\right), \ldots, s\left(\theta_{\omega_J}\right)\right] \in \mathbb{C}^{\omega_J \times \omega_J}$ and $\psi_T = \left[s\left(\theta_1\right), \ldots, s\left(\theta_{d_h}\right), \ldots, s\left(\theta_{\omega_h}\right)\right] \in \mathbb{C}^{\omega_h \times \omega_h}$, $\theta_{d_J} = \dfrac{2d_J - \omega_J - 1}{\omega_J}$ with $d_J = 1, 2, \ldots, \omega_J$, and $\theta_{d_h} = \dfrac{2d_h - \omega_h - 1}{\omega_h}$ with $d_h = 1, 2, \ldots, \omega_h$. Owing to the limited amount of scatterers, the angular-domain representation demonstrates significant sparsity. This inherent sparsity has been effectively employed by several Compressive Sensing (CS)-based channel estimation approaches to address far-field channel estimation challenges.

(ii) Near-field channel

Unlike the far-field case, where a planar wavefront is considered, the near-field channel must be modeled by exploiting a spherical wavefront. Consequently, the far-field array response vectors need to be replaced with near-field array response vectors to precisely capture the features of near-field propagation. Moreover, the near-field channel is signified below,

$$Z_{near-field} = \sqrt{\frac{\omega_J \omega_h}{\varepsilon - 1}} \sum_{C_d=1}^{\varepsilon\omega} \hbar C_d G\left(N_{\kappa,C_d}, \theta_{\kappa,C_d}\right) G^H\left(N_{T,C_d}, \theta_{T,C_d}\right) \tag{6}$$

here, $\varepsilon_\omega = \varepsilon - \varepsilon_W$ signifies the count of near-field elements between all the ε paths. Moreover, the near-field array response vectors corresponding to the BS and the UE are symbolized by $\left(N_{\kappa,C_d}, \theta_{\kappa,C_d}\right)$ and $\left(N_{T,C_d}, \theta_{T,C_d}\right)$ correspondingly.

Far-field channels are classified by notable sparsity in the angular domain, while near-field channels exhibit pronounced sparsity in the polar domain. To express the near-field channel in the polar domain, it is crucial to first devise the corresponding polar-domain transformation matrices $Q_\kappa \in \mathbb{C}^{\omega_J \times \omega_J}$ and $Q_T \in \mathbb{C}^{\omega_h \times \omega_h}$. Using the transformation matrices Q_κ and Q_T, the polar-domain representation of the near-field channel, typified by $Z^{\beta}_{near-field} \in \mathbb{C}^{\alpha_J \times \alpha_h}$, can be articulated below:

$$Z_{near-field} = Q_\kappa Z^{\beta}_{near-field} \in Q^H_T \tag{7}$$

Additionally, the hybrid-field XL-MIMO channel Z is written as,

$$Z = Z_{far-field} + Z_{near-field} \tag{8}$$

$$Z = \psi_\kappa Z^{v}_{far-field} \psi^H_T + Q_\kappa Z^{\beta}_{near-field} \in Q^H_T \tag{9}$$

As shown in (9), the hybrid-field channel is composed of a superposition of far-field and near-field elements. As a result, if the number of propagation paths associated with every field region can be recognized, the far-field and near-field channels can be evaluated independently. These individually estimated components can then be integrated to reconstruct the complete hybrid-field channel.

4 Proposed Bitterling Swallow Fish Optimization Algorithm for Pilot-Aided Channel Estimation in Extremely Large-Scale-Multiple-Input-Multiple-Output Systems

In wireless communication systems, precise channel estimation is essential for reliable data transmission. This paper develops the DKN_BSwaFOA model for pilot-aided channel estimation in XL-MIMO systems. Initially, the system model of XL-MIMO is considered. At the transmitter, the input data/signal is subjected to S/P conversion first. Thereafter, pilot insertion is done, and the location of the pilot symbol is ideally selected utilizing BSwaFOA. Here, the BSwaFOA is designed by incorporating the HSO [26] and BFO [11]. Later, the IFFT [18] for converting the frequency domain signal to the time domain. Then, the CP is added to avoid ISI. After that, the signal is allowed for P/S conversion, and then, the signal is propagated over the hybrid field channel, where far field or near field coexist. At the receiver, S/P conversion is done, followed by CP removal. Later, the signal is subjected to FFT [27] to convert the signal back to the frequency domain. The signal is then converted back to serial form via Parallel to Serial (P/S) conversion and transmitted over a hybrid field channel, where near-field and far-field effects coexist. At the receiver, S/P conversion is done, followed by CP removal. Later, the signal is subjected to an FFT to convert the signal back to the frequency domain. Thereafter, P/S conversion is done, and the pilot-aided channel is estimated using DKN [28], which is trained using the proposed BSwaFOA. The pictorial view of DKN_BSwaFOA for pilot-aided channel estimation in XL-MIMO systems is portrayed in Fig. 2.

4.1 Transmitter

The input signal is first converted from S/P. Following this, pilot insertion is applied, and the location of the pilot symbol is optimally selected utilizing BSwaFOA. Later, the IFFT is used for converting the frequency domain signal to the time domain. A CP is added to minimize interference, followed by a P/S conversion for transmission. The signal propagates via the near-field and far-field

regions, with the Rayleigh distance marking the boundary among them, affecting how the signal behaves during transmission.

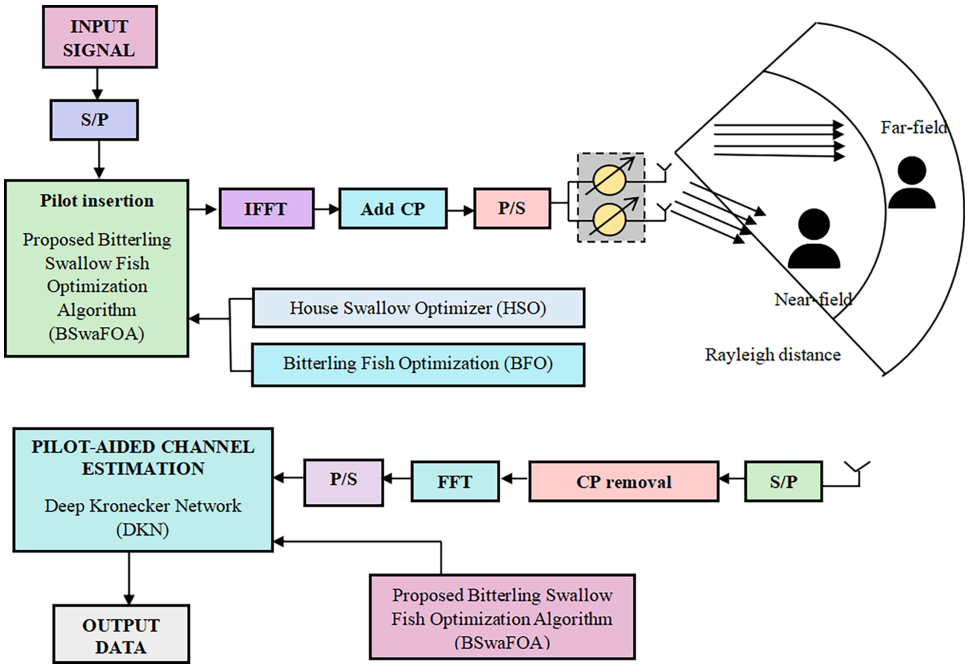

Figure 2: Systematic representation of the DKN_BSwaFOA for pilot-aided channel estimation in XL-MIMO systems

4.2 Select Optimal Location of Pilot Symbols Using Proposed BSwaFOA

Precise channel estimation heavily relies on the placement of pilot symbols within the transmitted data frame. Inappropriate pilot allocation can lead to poor channel estimation, minimizing the overall performance of the model. To address this, the devised BSwaFOA is utilized to select the optimum locations of pilot symbols. Here, the BSwaFOA is designed by incorporating the HSO [26] and BFO [11]. Moreover, the solution encoding, fitness function, and explanation of the BSwaFOA are elaborated in the ensuing subsections.

4.2.1 Solution Encoding

Solution encoding is crucial to signify candidate solutions in a format that the optimization algorithm can procedure. Encoding assists in defining and manipulating probable pilot locations systematically. This allows the algorithm to efficiently search, compare, and evolve solutions toward optimum pilot arrangements for enhanced channel estimation performance. Here, the solution is encoded as a sequence of 1, 2, 3, . . . , A', where A' indicates pilot estimation, and V' signifies the number of pilot symbols. The pictorial view of solution encoding is depicted in Fig. 3.

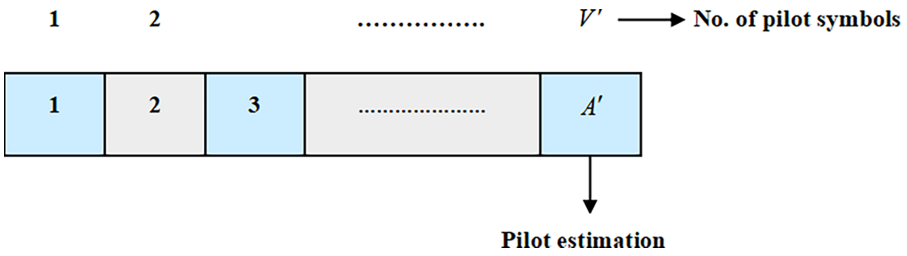

Figure 3: Schematic view of solution encoding

4.2.2 Fitness Function

The fitness function assesses the quality of every candidate pilot symbol arrangement during the optimization procedure. In this research, Bit Error Rate (BER) [29] is exploited for evaluating the fitness function. BER evaluates the proportion of incorrectly received bits to the overall transmitted bits, directly reflecting the precision of channel estimation. Further, the minimal BER represents the better performance, indicating the pilot symbol placement leads to more precise channel estimates and fewer transmission errors. The expression exploited for assessing the BER is designated beneath,

$$BER = \frac{No.of\ bit\ errors}{No.of\ transmitted\ bits} \tag{10}$$

4.2.3 Proposed BSwaFOA

The optimal location of pilot symbols is selected exploiting the designed BSwaFOA. Here, the BSwaFOA is newly established by the amalgamation of HSO [26], and BFO [11]. An innovative meta-heuristic algorithm, termed the HSO [26], is inspired by the house swallows' complex and adaptive behaviours. House swallows reveal complex flight patterns and social behaviours that enable them to adapt effectively to dynamic environments. The HSO is inspired by these natural behaviours to efficiently navigate complex search spaces. Employing their dynamic flight patterns, cooperative foraging, and navigational intelligence, HSO provides faster convergence, improved exploration and exploitation abilities, and optimized performance in solving complex optimization problems. Furthermore, the BFO [11] algorithm is a nature-inspired meta-heuristic based on the unique reproductive behavior of bitterling fish, which lay their eggs inside freshwater mussels for protection and survival. This behavior reflects intelligent cooperation, decision-making, and adaptation to environmental constraints. BFO utilizes these traits to balance exploration and exploitation in complicated search spaces. Further, the BFO achieves strong global search ability, robustness in avoiding local optima, and efficacy in solving high-dimensional and multimodal optimization issues. By assimilating the BFO and HSO, the devised BSwaFOA enhances the selection of optimum pilot symbol locations, leading to enhanced accuracy and efficacy. The mathematical stages of BSwaFOA are deliberated below,

Phase (i) Population initialization

BSwaFOA is a population-based optimization approach in which each house swallow designates a potential solution that is continuously refined throughout the optimization procedure. In this technique, the collective set of house swallows is mathematically signified as a population matrix. During the initialization stage, the locations of these swallows i.e., candidate solutions, are arbitrarily

initialized to start the search process. Moreover, the population matrix is expressed in Eq. (11).

$$E = \begin{bmatrix} E_1 \\ \vdots \\ E_I \\ \vdots \\ E_b \end{bmatrix}_{b\times dim} = \begin{bmatrix} j_{1,1} & \cdots & j_{1,\gamma} & \cdots & j_{1,dim} \\ \vdots & \ddots & \vdots & \ddots & \vdots \\ j_{I,1} & \cdots & j_{I,\gamma} & \cdots & j_{I,dim} \\ \vdots & \ddots & \vdots & \ddots & \vdots \\ j_{b,1} & \cdots & j_{b,\gamma} & \cdots & j_{b,dim} \end{bmatrix}_{b\times dim} \tag{11}$$

wherein, E_I specifies the position of I^{th} individual, dim designates the decision variable count, b exemplifies the total number of possible solutions, $j_{I,\gamma}$ typifies the decision variable of I^{th} individual at γ^{th} dimension, and the population of the house swallow is symbolized by E.

Phase (ii) Fitness evaluation

After initializing the house swallow population, their fitness is evaluated utilizing expression (3), and the solution with the minimum fitness value is contemplated the best candidate.

Phase (iii) Roosting and hovering

Firstly, house swallows detect potential hunting areas and hover within them. Their next action is determined by a random value D_1 in the range (0, 1). If $D_1 < 0.5$, they proceed to stage 1, exhibiting roosting or hovering behavior. If $D_1 > 0.5$, they transition to stage 2, adopting two preying strategies. Hovering plays a vital role by allowing precise insect capture through stationary flight, thereby optimizing predation efficacy. Swallows also hover near nests to feed their young, showcasing adaptive behavior. When an area becomes unsuitable, they relocate to more promising regions, reflecting strong global search capabilities. Position updates are expressed by Eqs. (12) and (13); if the new location attains a better objective value, it replaces the previous one, indicating the discovery of a more favourable hunting spot.

$$j_{I,\gamma}^{L1} = \begin{cases} j_{I,\gamma} + (1+\cos D_2) \times \left(best_\gamma - j_{I,\gamma}\right), & \Omega_{c_1} < \Omega_I \\ j_{I,\gamma} + B \times \mu \times \left(j_{c_1,\gamma} - j_{I,\gamma}\right), & else \end{cases} \tag{12}$$

where, a randomly generated number in the range of 0 to 1 is designated by D_2, Ω_I typifies the objective function for I^{th} house swallow, $best$ symbolizes the ideal location identified by the house swallows on the basis of the value of objective function, $j_{I,\gamma}^{L1}$ designates I^{th} house swallow in γ^{th} dimension at phase 1, the parameter $B = 2 \times randn\,(1, \dim) - 1$, j_{c_1}, $c_1 \in \{1, 2, \ldots, b\}$, $c_1 \neq I$ indicates the position of an arbitrarily chosen point that influences the migration direction of the I^{th} house swallow and Ω_{c_1} designates the associated objective function value at that point. The location update mechanism is carried out on the basis of Eq. (13).

$$E_I = \begin{cases} E_I^{L1}, & \Omega_I^{L1} < \Omega_I \\ ub + lb - j_{I,\gamma}^{L1}, & \Omega_{OBL} < \Omega_I < \Omega_I^{L1} \\ E_I, & \Omega_I < \Omega_{OBL} \end{cases} \tag{13}$$

here, the minimal and maximal value of the search space is symbolized by lb and ub, E_I^{L1} indicates a new position generated by I^{th} house swallow in phase 1 with Ω_I^{L1} is its fitness function, the expression $ub + lb - j_{I,\gamma}^{L1}$ specifies a strategy based upon in adversarial learning, where Ω_{OBL} indicates the corresponding objective value. In addition, the μ parameter is derived by modeling the nesting behaviour of the

domestic house swallow, and is articulated in Eq. (14).

$$\mu = \left(F - \exp\left(\frac{L-1}{\max\_iter}\right)\right)^{\frac{1}{n}} * \cos\left(2 * \pi * D_3\right) \tag{14}$$

where, D_3 signifies a random number from 0 to 1, $\max\_iter$ indicates the maximum iteration limit, L designated current iteration count, and the value of n is fixed at 8.

Phase (iv) Preying

House swallows reveal highly agile flight dynamics, allowing rapid manipulation across numerous directions within their environment. As insectivorous birds, they provide significantly to pest control by targeting species, namely flies, moths, and mosquitoes, hence satisfying a crucial ecological function. Remarkably, a single nest may account for the removal of millions of insects over the season of a summer, assisting ecosystem stability. Their accurate and high-velocity predation, both aerially and near aquatic surfaces, has led to the development of mathematical frameworks characterizing their hunting behavior, as designated in Eqs. (15) and (16).

$$j_{I,\gamma}^{L_2} = best_\gamma - K_1 * \ell_{levy} \times \left(j_{I,\gamma} - best_\gamma\right) \tag{15}$$

$$E_I = \begin{cases} E_I^{L_2}, & \Omega_I^{L_2} < \Omega_I \\ E_I, & else \end{cases} \tag{16}$$

here, $E_I^{L_2}$ indicates a new position generated by I^{th} house swallow in phase 2 with $\Omega_I^{L_2}$ is its fitness function, $Levy\,(\cdot)$ signifies the house swallow's levy flight, K_1 designates the value that adapts with iteration count and $j_{I,\gamma}^{L_2}$ specifies I^{th} house swallow in γ^{th} dimension at phase 2.

$$\ell_{levy} = Levy\,(\dim) \tag{17}$$

Further, K_1 alters iteratively, adjusting its value on the basis of the current iteration number, and is articulated as follows,

$$K_1 = 1 - \frac{L}{\max\_iter} \tag{18}$$

wherein, $Levy\,(dim())$ denotes levy flight of house swallows, which is stated by,

$$Levy\,(\dim) = 0.01 \times \frac{U}{|p|^{\frac{1}{z}}} \tag{19}$$

From the expression, the values of U and p are independently sampled according to Gaussian probability distributions, especially $U \sim N\left(0, \sigma_U^2\right)$ and $p \sim N\left(0, \sigma_p^2\right)$, the descriptions of σ_U^2 and σ_p^2 correspond to Eq. (20).

$$\sigma_U = \left(\frac{\sin\left(\frac{\pi z}{2}\right) H\,(1+z)}{2\left(\frac{z-1}{2}\right) H\left(\frac{1+z}{2}\right) z}\right)^{\frac{1}{z}}, \sigma_p = 1 \tag{20}$$

where in, shape parameter and gamma function are indicated by z and H. Moreover, the shape parameter z ranges from [0, 2], and is fixed at 1.5.

In Eq. (15), assume $j_{I,\gamma}^{L_2}$ as $j_{I,\gamma}\,(L+1)$, and $j_{I,\gamma}$ as $j_{I,\gamma}\,(L)$, we get

$$j_{I,\gamma}\,(L+1) = best_{\gamma} - K_1 * \ell_{levy} \times \left(j_{I,\gamma}\,(L) - best_{\gamma}\right) \tag{21}$$

$$j_{I,\gamma}\,(L+1) = best_{\gamma} - K_1 * \ell_{levy} \times j_{I,\gamma}\,(L) + K_1 \times \ell_{levy} \times best_{\gamma} \tag{22}$$

BFO [11] is applied to enhance the performance and accuracy of the model. From BFO [11],

$$j_{I,\gamma}\,(L+1) = \begin{cases} V \cdot j_{I,\gamma}\,(L) + \left(j^{+} - V \cdot j_{I,\gamma}\,(L)\right) \cdot Y, & A \le g \\ V \cdot j_{I,\gamma}\,(L) + \left(j^{*} - V \cdot j_{I,\gamma}\,(L)\right) \cdot Y & A > g \end{cases} \tag{23}$$

wherein, the optimal solution is designated by j^{*}, g denotes the parameter, V signifies the step size or movement rate of the fish as it either techniques or escapes from the oyster, and random numbers among 0 and 1 is represented by Y and A, and j^{+} denotes an arbitrarily selected the most promising individual in the oyster population.

In Eq. (23), consider the condition (i), i.e., $A \le g$, the equation becomes

$$j_{I,\gamma}\,(L+1) = V \cdot j_{I,\gamma}\,(L) + \left(j^{+} - V \cdot j_{I,\gamma}\,(L)\right) \cdot Y \tag{24}$$

$$j_{I,\gamma}\,(L+1) = V \cdot j_{I,\gamma}\,(L) + j^{+} * Y - V \cdot j_{I,\gamma}\,(L) * Y \tag{25}$$

$$j_{I,\gamma}\,(L+1) = V \cdot j_{I,\gamma}\,(L)\,[1-Y] + j^{+} * Y \tag{26}$$

$$j_{I,\gamma}\,(L) = \frac{j_{I,\gamma}\,(L+1) - j^{+} * Y}{V \cdot [1-Y]} \tag{27}$$

Applying Eqs. (27) in (22), we get

$$j_{I,\gamma}\,(L+1) = best_{\gamma} - K_1 * \ell_{levy} \times \left[\frac{j_{I,\gamma}\,(L+1) - j^{+} * Y}{V \cdot [1-Y]}\right] + K_1 \times \ell_{levy} \times best_{\gamma} \tag{28}$$

$$\frac{j_{I,\gamma}\,(L+1)\left[V \cdot [1-Y] + K_1 * \ell_{levy}\right]}{V \cdot [1-Y]} = \frac{best_{\gamma}\,(V \cdot [1-Y]) + K_1 * \ell_{levy} * j^{+} * Y + K_1 \times \ell_{levy} \times best_{\gamma}\,(V \cdot [1-Y])}{V \cdot [1-Y]} \tag{29}$$

$$j_{I,\gamma}\,(L+1) = \frac{best_{\gamma}\,(V \cdot [1-Y]) + K_1 * \ell_{levy} * j^{+} * Y + K_1 \times \ell_{levy} \times best_{\gamma}\,(V \cdot [1-Y])}{\left[V \cdot [1-Y] + K_1 * \ell_{levy}\right]} \tag{30}$$

The Eq. (30) is the final updated equation for BSwaFOA.

Phase (v) Nesting

House swallows strategically build half-bowl mud nests on vertical surfaces near rivers or ditches, favouring regions with abundant food supply. Their nesting behavior is defined as follows:

$$j_{I,\gamma}^{L_3} = j_{I,\gamma} + K_2 * a * \left(j_{I,\gamma} - best_{\gamma}\right) \tag{31}$$

$$E_I = \begin{cases} E_I^{L_3}, & \Omega_I^{L_3} < \Omega_I \\ E_I, & else \end{cases} \tag{32}$$

wherein, $j_{I,\gamma}^{L_3}$ symbolizes I^{th} house swallow in γ^{th} dimension at third phase, and $E_I^{L_3}$ indicates new position generated by I^{th} house swallow in third phase with $\Omega_I^{L_3}$ is its fitness function.

a quantifies the house swallow's flight proficiency during nest construction, as stated in expression (33).

$$a = fly * \left|j_{I,\gamma} - best_{\gamma}\right| \tag{33}$$

$$fly = \frac{1}{x * K_2} \tag{34}$$

$$x = t * \frac{v^2}{R} \tag{35}$$

$$K_2 = 1 + \frac{L}{\max\_iter} \tag{36}$$

wherein, house swallows' weight and flight speed are designated as t and v. Further, R typifies the parameter fixed as $R = 0.2 + 1.8 * D_2$.

Phase (vi) Breeding

The reproductive stage of the optimization algorithm is stimulated by the breeding behavior of house swallows, which lay 4–5 eggs twice yearly with a 15-day incubation period. Despite nesting independently, they form colonies for mutual defense and vigilance. This behavior is stated in expression (37) employing a diffusion search model.

$$j_{I,\gamma}^{L4} = best_\gamma + \left(X_{dis} - best_\gamma\right) * (1 + 2\upsilon) \tag{37}$$

$$E_I = \begin{cases} E_I^{L4}, & \Omega_I^{L4} < \Omega_I \\ E_I, & else \end{cases} \tag{38}$$

here, the variable υ involves multiple arrays sampled from Gaussian distributions, X_{dis} symbolizes the matrix resulting from sorting group locations in ascending order of distance to the ideal nest location $best_\gamma$.

Phase (vii) Migration

House swallows are migratory birds that travel long distances to achieve appropriate wintering habitats. They migrate northward in spring from regions, namely Australia, India, and the Malay Archipelago, arriving in China by March–April and returning south by mid-September. During migration, flocks form V-shaped or linear formations led by strong individuals, minimizing energy use via aerodynamic drafting. This cooperative strategy conserves energy, optimizes efficacy, and increases survival by adaptively selecting the finest leader. The behavior is mathematically articulated as beneath:

$$j_{I,\gamma}^{L5} = \begin{cases} j_{I,\gamma} + S\,(0,\ 1) * \left(j_{I,\gamma} - J' * best_\gamma\right), & \Omega_{c_2} < \Omega_i \\ j_{I,\gamma} + S\,(0,\ 1) * \left(best_\gamma - J' * j_{I,\gamma}\right), & else \end{cases} \tag{39}$$

wherein, Ω_{c_2} exemplifies the fitness value of a randomly chosen individual from the population, and $S\,(0, 1)$ indicates Cauchy mutation.

$$E_I = \begin{cases} E_I^{L5} & \Omega_I^{L5} < \Omega_I \\ E_I & else \end{cases} \tag{40}$$

$$J' = 0.05 \times \frac{1 - \ln\,(L + 1)}{\ln\,(\max\_iter + 1)} \tag{41}$$

The Cauchy mutation operator $S\,(0, 1)$ exploits a one-dimensional Cauchy distribution, a continuous distribution with two parameters, as deliberated by the probability density function in expression (42).

$$i\,(G', R', k') = \frac{1}{\pi} \frac{q}{R'^2 + (G' - k')^2}, -\infty < G' < \infty \tag{42}$$

wherein, $R' = 1, k' = 0$, the probability density function regards its typical form, as specified in expression (43),

$$i(G', R', k') = \frac{1}{\pi}\frac{1}{G'^2 + 1}, -\infty < G' < \infty \tag{43}$$

Phase (viii) Termination

BSwaFOA is terminated after reaching the predefined maximum iterations, at which point the ideal solution is attained. Algorithm 1 outlines pseudocode of BSwaFOA.

Algorithm 1: Pseudocode of BSwaFOA

Input: The maximum iteration limit max_*iter*, count of populations b, and the problem space dimensionality R
Update: The ideal position and its respective optimal fitness function value
Initialize the population X of the populations
for $L = 1:$ max_*iter*
Updation of the ideal position of house swallows according to the fitness function value
for $I = 1: b$
if $D < 0.5$
Stage 1: Roosting and hovering
Update the position of house swallows employing expression (12) and expression (13)
else
Phase 2: Preying
Apprise the house swallows' location utilizing Eq. (30) and expression (16)
end
Phase 3: Nesting
Apprise the house swallows' location using Eqs. (31) and (32)
Phase 4: Breeding
Apprise the house swallows' location employing Eqs. (37) and (38)
Phase 5: Migration
Update the house swallows' location employing Eqs. (39) and (40)
end
Retain the ideal candidate solutions up to this point
end
Output: This optimal fitness function value and respective optimal position

The pilot insertion is carried out utilizing the devised BSwaFOA. This algorithm incorporates the exploration ability of HSO with the exploitation ability of BFO. By amalgamating both approaches, BSwaFOA attains a balanced search capability, leading to more precise and effective pilot symbol placement for optimized channel estimation.

4.3 Receiver Phase

At the receiver phase, the incoming signal is initially converted from S/P. The CP is removed to eliminate ISI and restore the actual symbol structure. The signal is then transformed from the time domain, exploiting FFT. Thereafter, P/S conversion is applied. Further, the pilot aided channel

estimation is then carried out exploiting DKN [28], which is trained using BSwaFOA. At last, the receiver outputs the recovered data, accomplishing the communication procedure.

4.4 Pilot Aided Estimation Using DKN

Pilot-aided estimation is an approach exploited in wireless communication to evaluate the channel state by inserting known symbols, termed pilot symbols, into the transmitted signal. At the receiver, these known symbols assist in precisely estimating the channel's effect on the transmitted data, enabling better signal recovery and enhanced overall performance. In this research, the pilot aided channel is estimated using the DKN framework [28], which is tuned using the proposed BSwaFOA. Moreover, the BSwaFOA is designed by the assimilation of BFO [11], and HSO [26].

4.4.1 Architecture of DKN

Current channel observation ω' is fed as an input to DKN. DKN [28] is a technique that minimizes the difficulties of limited sample sizes in pilot-aided channel estimation, assisting more reliable and robust learning from scarce training data. By exploiting a Kronecker product structure, DKN efficiently incorporates numerous feature spaces, including pilot signals and channel state information, to capture complex interactions inherent in wireless channels. This capability permits DKN to model the complex relationships between multiple features, such as temporal and spatial channel variations, optimizing the accuracy of channel estimation. In addition, DKN's flexibility extends to processing channel data signified in both matrix and tensor forms, making it well-suited for diverse pilot-aided estimation scenarios.

Contemplate, P samples with matrix-complex data $e \in \mathbb{R}^{\nu \times q}$ and $u_{\eta'}$ scalar responses, $\mu' = 1, \ldots, P$. Considering $u_{\eta'}$ consistent the generalized linear model delineated beneath;

$$u_{\eta'}|e \sim O\left(u_{\eta'}|e\right) = \vartheta\left(u_{\eta'}\right) \exp\left\{u_{\eta'} \langle e, \beta' \rangle - Y'\left(\langle e, \beta' \rangle\right)\right\} \tag{44}$$

wherein, target unknown coefficient matrix is symbolized by $\beta' \in \mathbb{R}^{\nu \times q}$, and probability is indicated as O. Further, $\vartheta(\cdot)$ and $Y'(\cdot)$ specifies known univariate functions. Given a known link function $C'(\cdot)$, the model in expression (45) can be further employed to derive additional potential design variables.

$$C'\left(\mathrm{E}\left(u_{\eta'}\right)\right) = \langle e, \beta' \rangle \tag{45}$$

To signify the coefficient β', a rank-f Kronecker product decomposition involving m' (≥ 2) factors is specified below,

$$\beta' = \sum_{r=1}^{f} u'^{r}_{m'} \otimes r^{r}_{m'-1} \otimes \cdots \otimes u'^{r}_{1} \tag{46}$$

where, $u'^{r}_{m'r} \in L'^{\nu_o \times q_o}$ signifies unknown matrices, $o = 1, \ldots, m'$; $r = 1, \ldots, f$, and the dimension of u'^{r}_{o} is not known. Though, specified features of the Kronecker product, they definitely vital to satisfy $\nu = \prod_{o=1}^{m'} \nu_o$ and $q = \prod_{o=1}^{m'} q_o$. For any matrices $u'_{o'}, \ldots, u'_{o''}$ with $o' \geq o''$.

$$u'_{o'} \otimes u'_{o'-1} \otimes \cdots \otimes u'_{o''} = \bigotimes_{o=o''}^{o''} u'_{f} \tag{47}$$

Consequently, expression (47) can be written as,

$$\beta' = \sum\nolimits_{r=1}^{f} \otimes_{o=I}^{1} u'^{r}_{o} \tag{48}$$

The output gained from DKN is symbolized by $M_{r'}^{'}$ and the pictorial view of DKN is portrayed in Fig. 4.

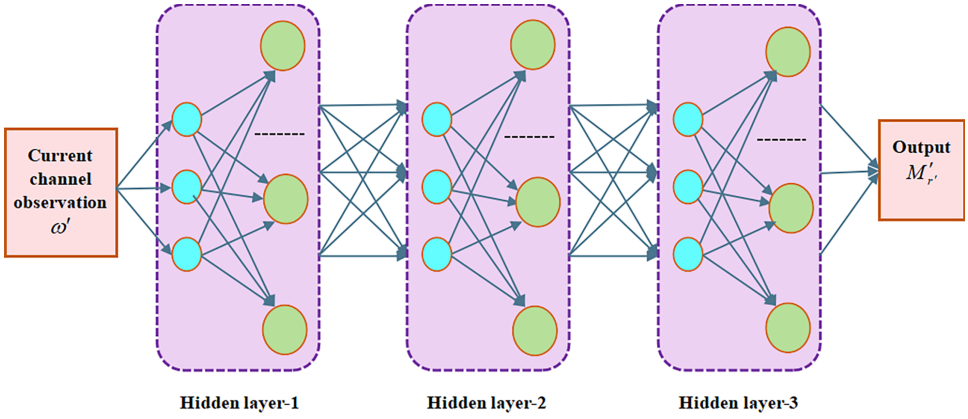

Figure 4: Structure of DKN technique

4.4.2 Training of DKN Using BSwaFOA

The effectualness of DKN in the pilot-aided channel estimation is enhanced by optimally modifying the parameters, exploiting BSwaFOA. In this case, the BSwaFOA is developed by the incorporation of HSO [26], and BFO [11]. An innovative meta-heuristic algorithm, termed the HSO [26], which is inspired by the house swallows' complex and adaptive behaviours. At the same time, the BFO [11] algorithm is a nature-inspired meta-heuristic based on the unique reproductive behavior of bitterling fish, which lay their eggs inside freshwater mussels for protection and survival. The HSO is assimilated with BFO to optimize the convergence speed and solution optimality. The corresponding algorithmic stages are systematically elaborated in Section 4.2.3, wherein the updated equation of BSwaFOA is specified beneath,

$$j_{I,\gamma}\left(L+1\right)=\frac{best_{\gamma}\left(V\cdot\left[1-Y\right]\right)+K_{1}*\ell_{levy}*j^{+}*Y+K_{1}\times\ell_{levy}\times best_{\gamma}\left(V\cdot\left[1-Y\right]\right)}{\left[V\cdot\left[1-Y\right]+K_{1}*\ell_{levy}\right]} \tag{49}$$

i) ***Fitness function:*** The optimal solution of the BSwaFOA is examined by exploiting the Mean Square Error (MSE) while tuning the DKN. The minimal fitness is contemplated for calculating the optimal solution, and the equation is stated below,

$$MSE=\frac{1}{\Phi}\sum_{r'=0}^{\Phi}\left(M'^{*}_{r'}-M_{r'}^{'}\right)^{2} \tag{50}$$

wherein, the overall count of training samples is designated by Φ, the expected outcome is specified as $M_{r'}^{'*}$ and the obtained output from DKN is represented as $M_{r'}^{'}$.

5 Results and Discussion

The supremacy of the DKN_BSwaFOA technique in pilot-aided channel estimation in XL-MIMO is assessed in contrast to the numerous prevailing techniques in this section. In addition, analysis is performed on the basis of ablation, Signal-to-Interference-plus-Noise Ratio (SINR), and the number of users based on various measures, and they are exemplified in the sections below.

5.1 Experimental Setup

The implementation of the DKN_BSwaFOA approach used in estimating the pilot-aided channel estimation is done in Python 3.9.11 with simulation.

5.2 Experimental Parameters

The simulation parameters of the XL-MIMO network and the experimental settings of the DKN and BSwaFOA are provided in this section.

(i) Experimental setting

In Table 2, the experimental settings of the DKN and BSwaFOA techniques are delineated.

(ii) Simulation parameter

The simulation parameter of the XL-MIMO network is indicated in Table 3.

Table 2: Experimental settings of the BSwaFOA and DKN

BSwaFOA		DKN	
Parameters	*Range*	*Parameters*	*Range*
Maximum iteration max _*iter*	500	Strides	2
Population size E	50	Batch size	16
Random number D_1	(0, 1)	Activation	Softmax
Lower bound *lb*	−10	Kernel size	(3, 3)
Decision variable	30	Loss	Categorical cross entropy
Random number D_2	(0, 1)	Dropout	0.3
Upper bound *ub*	10	Epoch	100
Random number D_3	(0, 1)	Optimizer	BSwaFOA

Table 3: Simulation parameter of XL-MIMO

Parameters	*Range*
Number of subcarriers	256
User Equipment (UE) density	100 UE/km^2
Network radius	1000 m
Number of OFDM Symbols	14
SBS transmission power	5 W
Number of UEs	400
Base station density	10 BS/km^2
Simulation channels	Nakagami, Rician, and Rayleigh
Size of modulation constellation	64
Number of SBSs	30

5.3 Performance Indicators

The indicators, such as RMSE, MSE, and BER, are considered for assessing the effectiveness of the DKN_BSwaFOA model, and they are described below.

(i) BER: The ratio of the amount of incorrectly received bits to the whole amount of transmitted bit in a communication system is referred as BER, and it is represented in Eq. (10).

(ii) MSE: The average squared difference between the estimated channel response and the actual channel response attained using the pilot symbols is quantified by MSE, which is written as,

$$MSE = \frac{1}{h'}\sum_{r'=1}^{h'}\left(M_{r'}' - M_{r'}'^{*}\right)^2 \tag{51}$$

here, h' designates the number of samples, $M_{r'}'$ specifies the true value and $M_{r'}'^{*}$ typifies the predicted value.

(iii) RMSE: The square root of the MSE is referred to as RMSE, and it is designated by the below-specified expression.

$$RMSE = \sqrt{\frac{1}{h'}\sum_{r'=1}^{h'}\left(M_{r'}' - M_{r'}'^{*}\right)^2} \tag{52}$$

5.4 Simulation Results

The simulation result of the DKN_BSwaFOA technique at simulation time 8.13 s is illustrated in Fig. 5. Moreover, the network includes user devices, BS, and transceivers. Here, the BS communicates with multiple transceivers, and the users are represented in various colors. The red dashed lines indicate the interference from pilot contamination, while the red line represents the transmission of estimated channel data among the BS and transceivers.

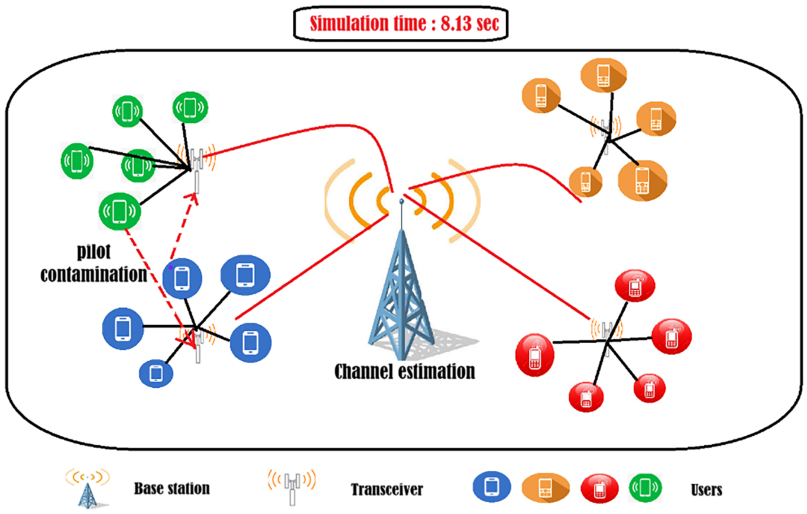

Figure 5: Simulation result of DKN_BSwaFOA

5.5 Experimental Analysis

Ablation analysis, analysis based on varying channels, comparative analysis based on SINR, and number of users, computational complexity analysis, and network performance analysis are performed to examining the superiority of the newly formulated DKN_BSwaFOA technique. Furthermore, the detailed assessment of the newly devised technique with other baseline methods is explicated below.

5.5.1 Ablation Analysis

To validate the contribution of the optimization process, an ablation study is carried out to evaluate the performance of the proposed DKN model with and without the BSwaFOA optimization technique. In Fig. 6, the ablation analysis performed to demonstrating the efficacy of the proposed DKN technique with optimization and without optimization is depicted. In Fig. 6a, the investigation of DKN in terms of RMSE with and without BSwaFOA is specified. Here, the RMSE value figured by DKN and DKN+BSwaFOA when considering Energy per bit to Noise power spectral density ratio (Eb/No) of 9 dB is 0.045 and 0.009. The BER-based analysis of the DKN with and without BSwaFOA is specified in Fig. 6b. The value of BER recorded by DKN and DKN+BSwaFOA at Eb/No of 8 dB is 0.007 and 0.002. Fig. 6c designates the BER assessment of DKN both with and without BSwaFOA. When assuming Eb/No of 7 dB, the MSE value measured by DKN is 0.025, and DKN+BSwaFOA is 0.003. This shows that a better performance is yielded when considering the optimization technique. From the results, it is evident that integrating BSwaFOA with DKN achieves lower RMSE, BER, and MSE values. This confirms that the optimization technique effectively improves channel estimation performance in XL-MIMO systems.

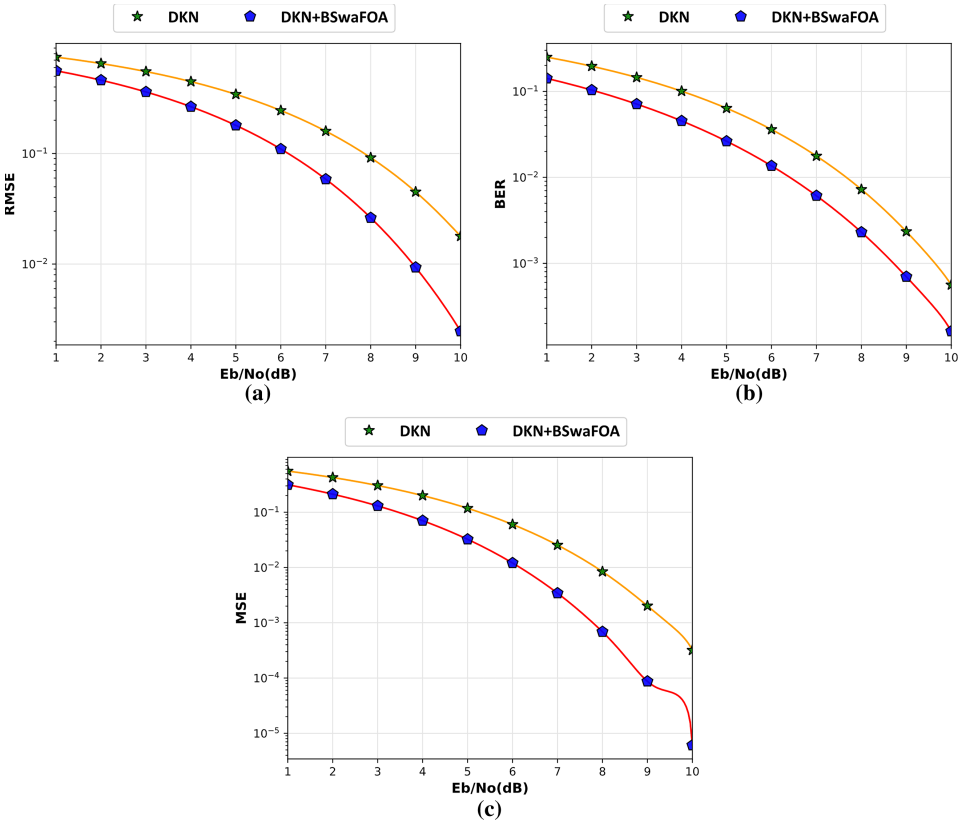

Figure 6: Ablation assessment of the DKN_BSwaFOA (**a**) RMSE, (**b**) BER, and (**c**) MSE

5.5.2 Analysis Based on Varying Channel

The assessment of the DKN_BSwaFOA technique by considering numerous channels, like Rayleigh, Rician, and Nakagami, is specified in Fig. 7. The estimation of the DKN_BSwaFOA in terms of RMSE is indicated in Fig. 7a. At Eb/No of 10 dB, the RMSE calculated by Nakagami+DKN _BSwaFOA, Rician+DKN_BSwaFOA, and Rayleigh+DKN_BSwaFOA is 0.006, 0.004, and 0.002. Fig. 7b delineates the examination of the DKN_BSwaFOA regarding BER. Here, the BER quantified by Nakagami+DKN_BSwaFOA, Rician+DKN_BSwaFOA, and Rayleigh+DKN_BSwaFOA for Eb/No of 8 dB is 0.006, 0.004, and 0.002. In Fig. 7c, the examination of the DKN_BSwaFOA regarding MSE is specified. When considering Eb/No of 7 dB, the MSE computed by Nakagami+DKN_BSw aFOA is 0.016, Rician+DKN_BSwaFOA is 0.011, and Rayleigh+DKN_BSwaFOA is 0.003. It is observed that the DKN_BSwaFOA method acquires more precise channel estimation and better system performance in the Rayleigh channel.

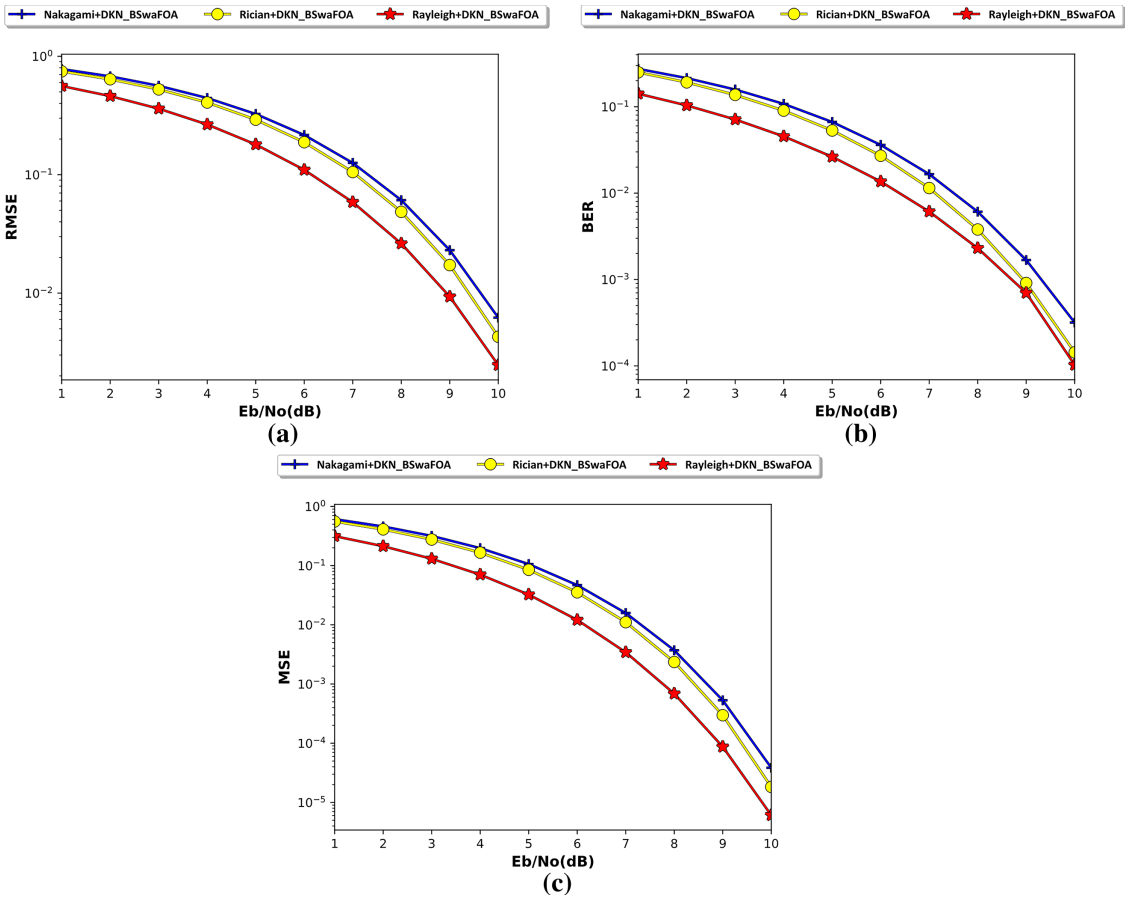

Figure 7: Analysis of DKN_BSwaFOA by varying channels (**a**) RMSE, (**b**) BER, and (**c**) MSE

5.5.3 Comparative Analysis

Different existing techniques, such as BPD [20], P-MSRDN [21], C-XLCNet [23], and SBL-GNN [25] employed for pilot aided channel estimation process are compared with the newly developed DKN_BSwaFOA approach for evaluating the superiority of the method. The examination of the

DKN_BSwaFOA approach by changing the number of users and SINR on the basis of different metrics is exemplified in the section below.

(i) By varying SINR

In Fig. 8, the examination of the DKN_BSwaFOA by varying SINR based on several measures is exemplified. Fig. 8a specifies the valuation of DKN_BSwaFOA performance using RMSE. Here, the DKN_BSwaFOA recorded the RMSE of 0.004 for the SINR of 9 dB, while the baseline methods, including BPD, P-MSRDN, C-XLCNet, and SBL-GNN, calculated the RMSE of 0.073, 0.025, 0.006, and 0.007. The BER-based assessment of the DKN_BSwaFOA is illustrated in Fig. 8b. At an SINR of 6 dB, the BER values measured by BPD, P-MSRDN, C-XLCNet, SBL-GNN, and DKN_BSwaFOA is 0.062, 0.030, 0.012, 0.011, and 0.004. In Fig. 8c, the graph drawn between the SINR and MSE is plotted. The value of MSE when assuming SINR 8 dB for BPD are 0.026, P-MSRDN is 0.008, C-XLCNet is 0.003, SBL-GNN is 0.002, and DKN_BSwaFOA is 0.001.

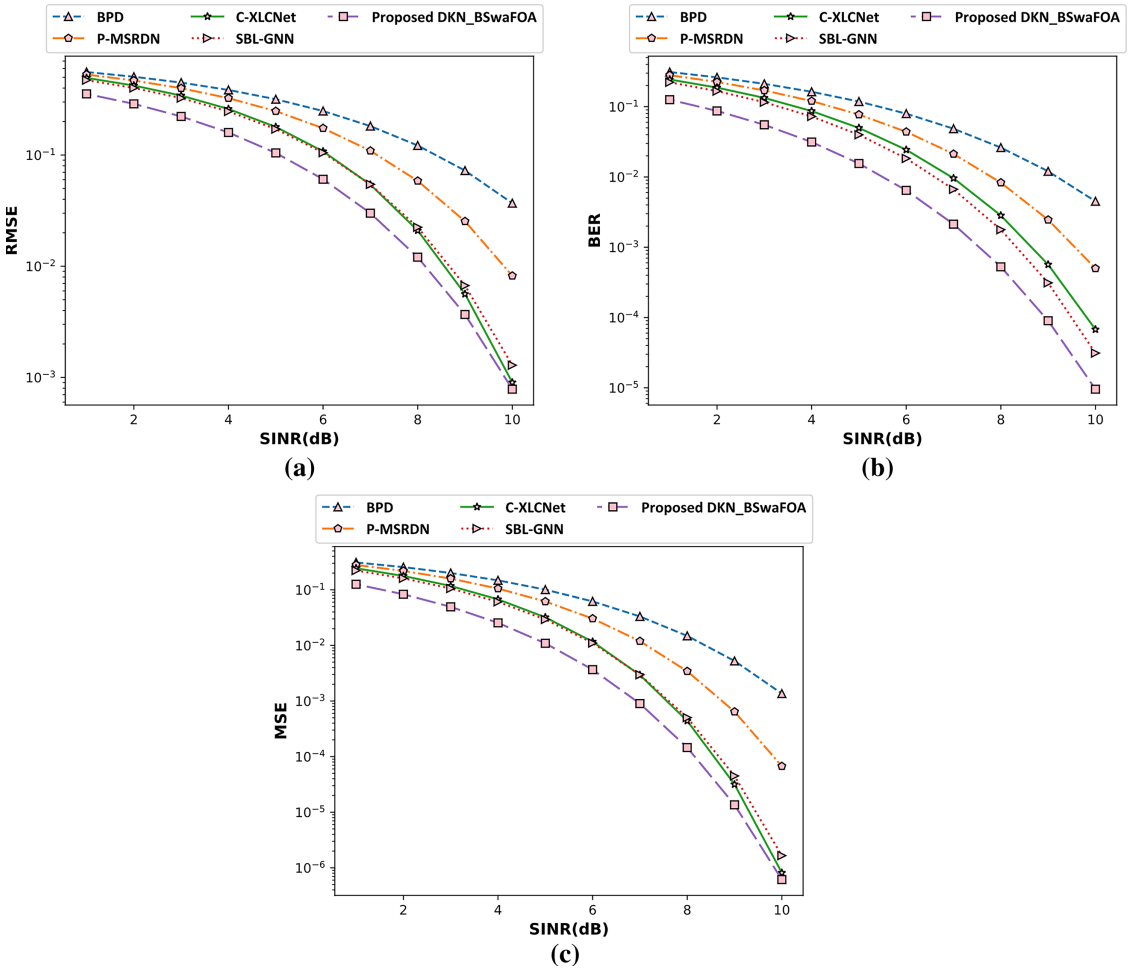

Figure 8: Analysis of DKN_BSwaFOA by varying SINR (**a**) RMSE, (**b**) BER, and (**c**) MSE

(ii) By varying the number of users

Fig. 9 portrays the examination of the DKN_BSwaFOA by altering the number of users based on several measures. The graph drawn amongst the number of users and RMSE is illustrated in Fig. 9a.

When considering the number of users as 90, the RMSE value measured by BPD, P-MSRDN, C-XLCNet, SBL-GNN, and DKN_BSwaFOA is 0.736, 0.718, 0.616, 0.526, and 0.503. Fig. 9b specifies the BER-based assessment of the DKN_BSwaFOA model. Here, the DKN_BSwaFOA recorded the BER of 0.233 for 80 users, while the baseline methods, including BPD, P-MSRDN, C-XLCNet, and SBL-GNN, gained the RMSE of 0.483, 0.500, 0.351, and 0.253. In Fig. 9c, the valuation of DKN_BSwaFOA performance using MSE metrics is plotted. The value of MSE when assuming 100 users by BPD is 0.736, P-MSRDN is 0.718, C-XLCNet is 0.616, SBL-GNN is 0.526, and DKN_BSwaFOA is 0.503.

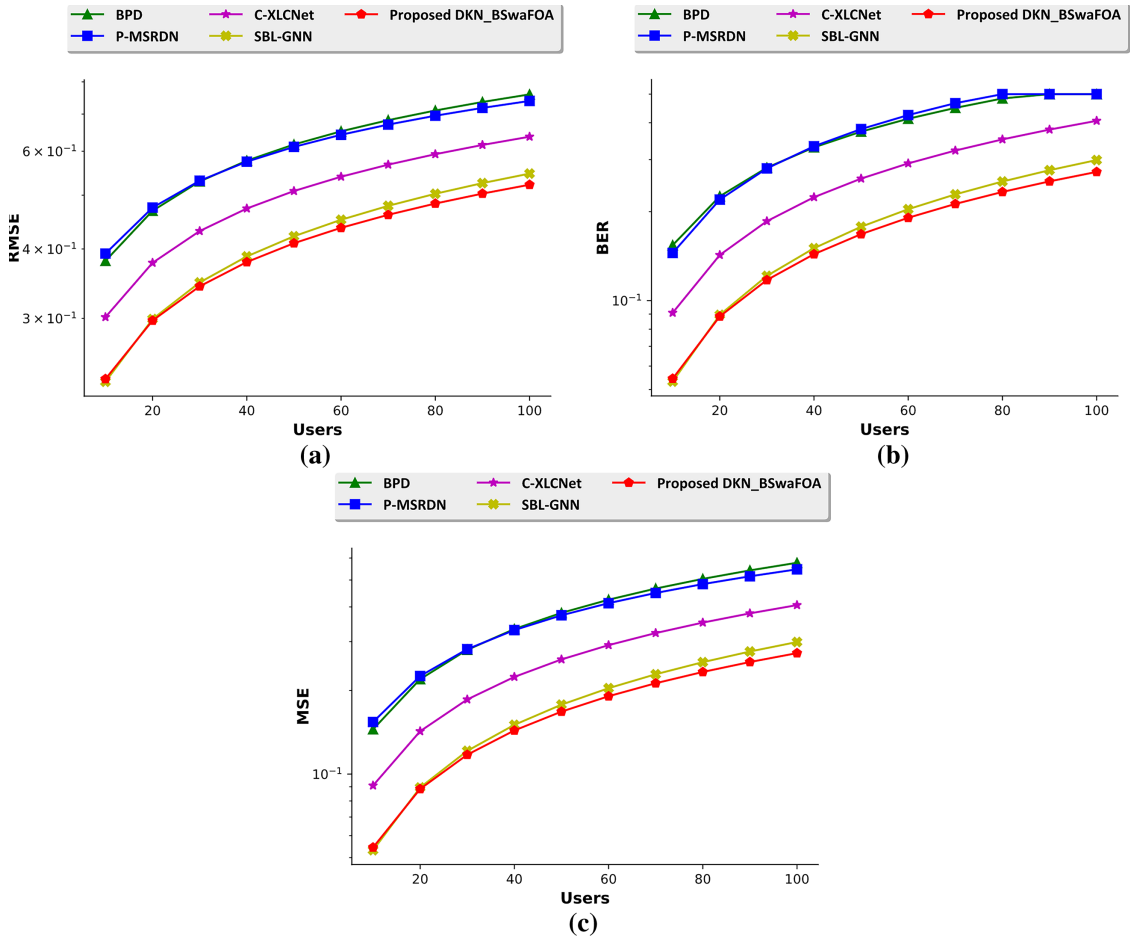

Figure 9: Analysis of DKN_BSwaFOA by varying number of users (**a**) RMSE, (**b**) BER, and (**c**) MSE

5.5.4 Computational Complexity Analysis

Table 4 presents the computational complexity comparison of various channel estimation methods in terms of computational time and memory. The proposed DKN_BSwaFOA achieves the lowest computational time of 20.47 s and memory usage of 10.50 MB among all compared models. This efficiency results from the BSwaFOA's optimal pilot selection, which reduces redundant computations, and the lightweight structure of DKN, which minimizes parameter redundancy. Consequently, the

proposed method ensures faster processing and lower resource consumption, making it well-suited for real-time XL-MIMO implementations.

Table 4: Computational complexity analysis

Methods	BPD	P-MSRDN	C-XLCNet	SBL-GNN	Proposed DKN_BSwaFOA
Computational time (s)	43.00	36.00	29.99	27.00	**20.47**
Memory (MB)	20.50	18.60	16.40	13.60	**10.50**

5.5.5 Simulation Results for 6G Networks

The applicability of the proposed DKN_BSwaFOA model for 6G networks is evaluated using the simulation parameters summarized in Table 3. The network performance is assessed in terms of energy efficiency and throughput, as illustrated in Fig. 10. The energy efficiency analysis is provided in Fig. 10a. When considering 100 users, the energy efficiency of the simulated 6G network is 80.00, 82.18, 86.17, 90.15, and 92.15 Mbits/Joule using BPD, P-MSRDN, C-XLCNet, SBL-GNN, and DKN_BSwaFOA. The results clearly indicate that the proposed model attains the highest energy efficiency among all compared methods. Fig. 10b denotes the throughput analysis. The throughput obtained by the BPD, P-MSRDN, C-XLCNet, SBL-GNN, and DKN_BSwaFOA is 86.89, 90.00, 93.00, 95.78, and 97.89 Mbps, when considering 100 users. It is observed that the throughput increases with the number of users up to the network's capacity limit, and the proposed DKN_BSwaFOA consistently achieves the highest throughput, demonstrating its superior data transmission capability and scalability for 6G environments. The simulation outcomes clearly show that the proposed DKN_BSwaFOA model delivers better energy efficiency and higher throughput than the existing methods. These results suggest that the model can make 6G networks more efficient and reliable by optimizing resource use and improving data transmission performance.

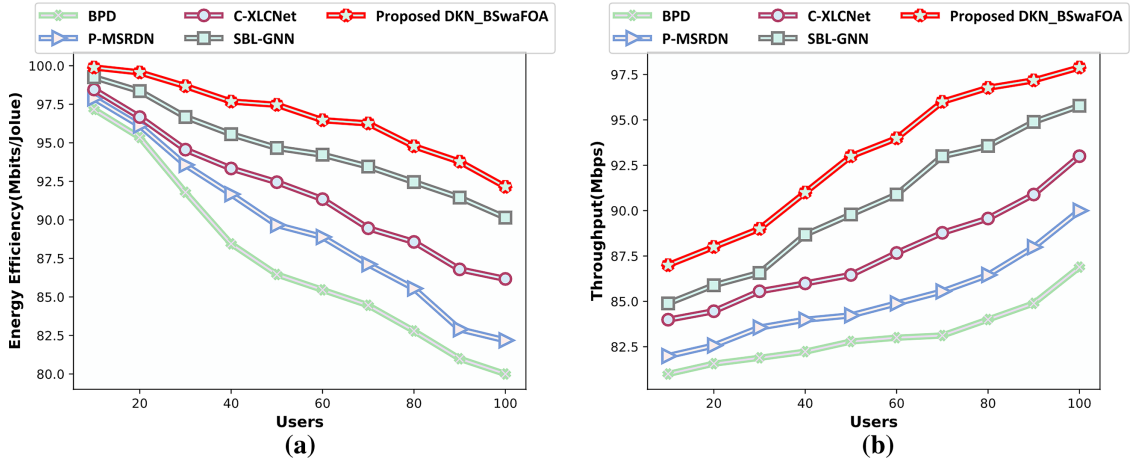

Figure 10: Simulation results for 6G networks based on (**a**) Energy efficiency, (**b**) Throughput

5.6 Summary

The comparative discussion of the DKN_BSwaFOA technique with respect to various measures for 70 users and SINR 7 dB is portrayed in Table 5. It is found that, for SINR 7 dB, the

DKN_BSwaFOA method computed a minimum RMSE, BER, and MSE of 0.030, 0.002, and 0.001. Further, the RMSE value quantified by the prevailing techniques, including BPD, P-MSRDN, C-XLCNet, and SBL-GNN, are 0.182, 0.109, 0.109, and 0.054, whereas the BER recorded by these approaches is 0.049, 0.021, 0.010, and 0.007. Additionally, the MSE calculated by the BPD is 0.033, P-MSRDN is 0.012, C-XLCNet is 0.003, and SBL-GNN is 0.003. Hence, the newly developed DKN_BSwaFOA approach obtained better consequences than other baseline techniques. Here, the DKN model is tuned utilizing the BSwaFOA, which is formulated by unifying the HSO and BFO models. Moreover, the BSwaFOA enhanced the overall optimization performance. Besides, the DKN, which is empowered by the adaptive learning capability of BSwaFOA, offered more robust and precise channel estimates. Hence, the DKN_BSwaFOA ensured a lower error rate and better adaptability.

Table 5: Comparative discussion of DKN_BSwaFOA

Metrics	BPD	P-MSRDN	C-XLCNet	SBL-GNN	Proposed DKN_BSwaFOA
By varying SINR					
RMSE	0.182	0.109	0.054	0.054	**0.030**
BER	0.049	0.021	0.010	0.007	**0.002**
MSE	0.033	0.012	0.003	0.003	**0.001**
By varying number of users					
RMSE	0.683	0.670	0.568	0.478	0.461
BER	0.449	0.466	0.322	0.229	0.212
MSE	0.466	0.449	0.322	0.229	0.212

6 Conclusion

In wireless communication systems, precise channel estimation is essential for reliable data transmission. This research designs an innovative approach, DKN_BSwaFOA, for pilot-aided channel estimation in XL-MIMO systems. Primarily, the system model of XL-MIMO is considered. Primarily, the input signal undergoes S/P conversion at the receiver. Subsequently, pilot insertion is done, and the location of the pilot symbol is optimally selected using BSwaFOA. Later, the IFFT is used for converting the frequency domain signal to the time domain. Subsequently, a CP is added to mitigate ISI. The signal is then converted back to serial form via P/S conversion and transmitted over a hybrid field channel, where near-field and far-field effects coexist. At the receiver phase, the signal first undergoes S/P conversion, followed by CP removal. The resulting signal is then transformed back to the frequency domain through FFT. Later, P/S conversion is applied and then pilot-aided channel estimation is done utilizing DKN, which is trained with BSwaFOA. The experimental results demonstrated that the DKN_BSwaFOA method computed the minimum RMSE, BER, and MSE of 0.030, 0.002, and 0.001. Future work aims to include joint beamforming and power allocation strategies to enhance performance.

Acknowledgement: The authors would like to thank all individuals and institutions that contributed to this research.

Funding Statement: This research was partially financed by the National Natural Science Foundation of China Project (project ID: U25A20581) and financed by the Fujian Provincial Natural Science Foundation Project (project ID: 2024J011540, 2024CT018). The authors express their gratitude to Quanzhou University of Information Engineering, and the Artificial Intelligence and Sensing Technologies Research Center, University of Tabuk for its support in this research.

Author Contributions: Mian Muhammad Kamal: Conceptualization, Methodology, Writing—original draft and Investigation. Syed Zain Ul Abideen: Data curation, Investigation and Writing—review & editing. Yinsheng Luo: Supervision, Data curation and Project administration. Abdelrahman Hamza Hussein: Data curation and Software. Husam S. Samkari: Methodology, Writing—review & editing and Project administration. Mohammed F. Allehyani: Conceptualization, Data curation and Funding acquisition. Tianjun Ma: Supervision, Writing—review & editing, Project administration and Funding acquisition. All authors reviewed the results and approved the final version of the manuscript.

Availability of Data and Materials: The datasets used and/or analysed during the current study are available from the corresponding authors on reasonable request.

Ethics Approval: Not applicable.

Conflicts of Interest: The authors declare no conflicts of interest to report regarding the present study.

References

1. Tao Q, Li Z, Zhi K, Li S, Yuan W, Zaniboni L, et al. Survey on reconfigurable intelligent surface-assisted orthogonal time frequency space systems. IEEE Open J Veh Techno. 2025;6:1881–909. doi:10.1109/ojvt.2025.3573208.
2. Lei H, Zhang J, Wang Z, Xiao H, Ai B, Ornson EBJ. Near-field user localization and channel estimation for XL-MIMO systems: fundamentals, recent advances, and outlooks. IEEE Wireless Commun. 2025. doi:10.1109/mwc.010.2400237.
3. Jin Z, You L, Ng DWK, Xia X-G, Gao X. Near-field channel estimation for XL-MIMO: a deep generative model guided by side information. IEEE Trans Cogn Commun Netw. 2025. doi:10.1109/tccn.2025.3566047.
4. Yahya SM, Christophe CM, Afeef L, Arslan H. Novel PDP-guided blockage sensing and mitigation in near-field XL-MIMO systems. Authorea. 2025. doi:10.22541/au.174785217.74718460/v1.
5. Ye M, Liang X, Pan C, Xu Y, Jiang M, Li C. GAN based near-field channel estimation for extremely large-scale MIMO systems. IEEE Trans Green Commun Netw. 2024;9:304–16. doi:10.1109/tgcn.2024.3416617.
6. Xu W, Liu A, Zhao M-j, Caire G. Joint visibility region detection and channel estimation for XL-MIMO systems via alternating MAP. IEEE Trans Signal Process. 2024;72:4827–42. doi:10.1109/tsp.2024.3479319.
7. Tang A, Wang J-B, Pan Y, Zeng C, Chen Y, Yu H, et al. Spatially non-stationary XL-MIMO channel estimation: a three-layer generalized approximate message passing method. IEEE Trans Signal Process. 2024;73:356–371. doi:10.1109/tsp.2024.3512575.
8. Lu Y, Dai L. Near-field channel estimation in mixed LoS/NLoS environments for extremely large-scale MIMO systems. IEEE Trans Commun. 2023;71(6):3694–707. doi:10.1109/tcomm.2023.3260242.
9. Yu W, Ma Y, He H, Song S, Zhang J, Letaief KB. Deep learning for near-field XL-MIMO transceiver design: principles and techniques. IEEE Commun Mag. 2025;63(1):52–8. doi:10.1109/mcom.001.2300829.
10. Deutschman BJB, Wilding T, Graber M, Witrisal K. XL-MIMO channel modeling and prediction for wireless power transfer. In: Proceedings of 2023 IEEE International Conference on Communications Workshops (ICC Workshops). IEEE; 2023.

11. Zareian L, Rahebi J, Shayegan MJ. Bitterling fish optimization (BFO) algorithm. Multimed Tools Appl. 2024;83(31):75893–926. doi:10.1007/s11042-024-18579-0.
12. Cui M, Dai L. Channel estimation for extremely large-scale MIMO: far-field or near-field? IEEE Trans Commun. 2022;70(4):2663–77. doi:10.1109/tcomm.2022.3146400.
13. Wei X, Dai L. Channel estimation for extremely large-scale massive MIMO: far-field, near-field, or hybrid-field? IEEE Commun Lett. 2021;26(1):177–81. doi:10.1109/lcomm.2021.3124927.
14. Zhang X, Wang Z, Zhang H, Yang L. Near-field channel estimation for extremely large-scale array communications: a model-based deep learning approach. IEEE Commun Lett. 2023;27(4):1155–9. doi:10.1109/lcomm.2023.3245084.
15. Cosovic I, Auer G. Capacity of MIMO-OFDM with pilot-aided channel estimation. EURASIP J Wirel Commun Netw. 2008;2007:032460. doi:10.1155/2007/32460.
16. Xu Y, Larsson EG, Jorswieck EA, Li X, Jin S, Chang T-H. Distributed signal processing for extremely large-scale antenna array systems: state-of-the-art and future directions. IEEE J Sel Top Signal Process. 2025;19:304–30. doi:10.1109/jstsp.2025.3541386.
17. Wu H, Lu L, Wang Z. Near-field channel estimation in dual-band XL-MIMO with side information-assisted compressed sensing. IEEE Trans Commun. 2024;73(2):1353–66. doi:10.1109/tcomm.2024.3445282.
18. Bhavani R, Sudhakar D. Design and implementation of inverse fast fourier transform for OFDM. Int J Sci Eng Appl. 2013;2(7):155–7.
19. Lu H, Zeng Y, You C, Han Y, Zhang J, Wang Z, et al. A tutorial on near-field XL-MIMO communications towards 6G. IEEE Commun Surv Tutor. 2024.
20. Cui M, Dai L. Near-field wideband channel estimation for extremely large-scale MIMO. Sci China Inf Sci. 2023;66(7):172303. doi:10.1007/s11432-022-3654-y.
21. Lei H, Zhang J, Xiao H, Zhang X, Ai B, Ng DWK. Channel estimation for XL-MIMO systems with polar-domain multi-scale residual dense network. IEEE Trans Veh Technol. 2023;73(1):1479–84. doi:10.1109/tvt.2023.3311010.
22. Liu S, Yu X, Gao Z, Xu J, Ng DWK, Cui S. Sensing-enhanced channel estimation for near-field XL-MIMO systems. IEEE J Sel Areas Commun. 2025;43(3):628–43. doi:10.1109/JSAC.2025.3531578.
23. Gao S, Dong P, Pan Z, You X. Lightweight deep learning based channel estimation for extremely large-scale massive MIMO systems. IEEE Trans Vehicular Technol. 2024;73(7):10750–4. doi:10.1109/tvt.2024.3364510.
24. Lei H, Zhang J, Wang Z, Ai B, Ng DWK. Hybrid-field channel estimation for XL-MIMO systems with stochastic gradient pursuit algorithm. IEEE Trans Signal Process. 2024;72:2998–3012. doi:10.1109/tsp.2024.3406348.
25. Tang A, Wang J-B, Pan Y, Zeng C, Chen Y, Yu H, et al. Channel estimation for XL-MIMO systems with decentralized baseband processing: integrating local reconstruction with global refinement. IEEE Trans Commun. 2025;73:9421–36. doi:10.1109/tcomm.2025.3564724.
26. Dong J, Wang L, Qiao S, Wang P, Tan X. House swallow optimizer: a new meta-heuristic algorithm and its application for DOA estimation of broadband signal in vector hydrophone array. IEEE Access. 2025;13:83717–37. doi:10.1109/ACCESS.2025.3569264.
27. Leitersdorf O, Boneh Y, Gazit G, Ronen R, Kvatinsky S. FourierPIM: high-throughput in-memory fast fourier transform and polynomial multiplication. Memories-Mater Devices Circ Syst. 2023;4:100034. doi:10.1016/j.memori.2023.100034.
28. Hajarathaiah K, Kolli CS, Tatireddy SR, Kumar MS, Radha VKR, Reddy VVK. Cascade Kronecker neuro-fuzzy network based influential node identification. Appl Soft Comput. 2025;175:113015. doi:10.1016/j.asoc.2025.113015.
29. Sarkar NI, Ammann R, Zabir SMS. Analyzing TCP performance in high bit error rate using simulation and modeling. Electronics. 2022;11:2254. doi:10.3390/electronics11142254.